Bioresource Technology 276 (2019) 127–132

Contents lists available at ScienceDirect

Bioresource Technology

journal homepage: www.elsevier.com/locate/biortech

Cr(VI) removal from aqueous solution using biochar modified with Mg/Al-layered double hydroxide intercalated with ethylenediaminetetraacetic acid

Danlian Huang[a,b,*], Caihong Liu[a,b], Chen Zhang[a,b], Rui Deng[a,b], Rongzhong Wang[a,b], Wenjing Xue[a,b], Hao Luo[a,b], Guangming Zeng[a,b], Qing Zhang[a,b], Xueying Guo[a,b]

[a] College of Environmental Science and Engineering, Hunan University, Changsha 410082, China
[b] Key Laboratory of Environmental Biology and Pollution Control (Hunan University), Ministry of Education, Changsha 410082, China

ARTICLE INFO

Keywords:
Biochar
Layered double hydroxides
Cr(VI)
Adsorption

ABSTRACT

In this study, the bamboo biomass loaded with ethylenediaminetetraacetic acid (EDTA) intercalated Mg/Al-layered double hydroxides (LDH) was calcined to obtain a novel nano-adsorbent (BC@EDTA-LDH), and BC@EDTA-LDH was used to remove hexavalent chromium (Cr(VI)) in aqueous solutions. The results showed that the interaction between LDH and Cr(VI) on biochar played a dominant part in adsorption. The LDH of Cr(VI) intercalation was successfully reconstructed after adsorption. Fourier transform infrared spectra and X-ray diffraction results confirmed the reconstruction of Mg/Al-LDH. LDH had sustained release effect on the solution. As the pH values increased, the electrostatic repulsion between $Cr_2O_7^{2-}$ and OH^- increased, and there existed competition for adsorption sites. The maximum adsorption capacity of Cr(VI) was 38 mg/g. The data was well-fitted with pseudo second-order model and Langmuir-Freundlich model. BC@EDTA-LDH showed a high adsorption capacity and was potentially suitable for removing heavy metals in wastewater.

1. Introduction

Nowadays, with the improvement of people's environmental awareness, heavy metal pollution has drawn more and more extensive attention in society (Gong et al., 2018; Huang et al., 2017a, 2016b). Excess heavy metals have adverse effects on ecological environment and human health (He et al., 2018; Li et al., 2018). Heavy metals can not be biodegraded and would cause harm to the human body through the bioaccumulation of the food chain (Gong et al., 2017; Xue et al., 2017). Cr(VI) has been identified as one of the human carcinogens by international cancer research institutions (Farrell et al., 1989). The pollution of chromium (Cr) is mainly caused by industry such as mining industry and smelting industry (Knott, 1996). Cr is usually existed in the natural environment in the forms of Cr(III) and Cr(VI). Cr(III), as one of the essential trace elements of a mammal, can regulate the levels of insulin and blood glucose (Xu and Zhao, 2007). Cr(III) mainly exists in the form of $Cr(OH)_3$ or Cr_2O_3, and it is easy to form a complex and stably exists in the sediment. The Cr(VI) toxicity is 100 times higher than Cr(III). Reportedly, long-term exposure of human skin to Cr(VI) wastewater is the origin of dermatitis and eczema. And the inhalation of Cr(VI) can cause sneezing, running nose, nosebleeds, ulcers, even lead to the kidneys and liver damage. In critical situations, Cr(VI) may could do harm to the human circulatory system or even threaten human life (Wang et al., 2000). Cr(VI) was highly mobile in water and soil (Fendorf et al., 2000). Cr(VI) in water is mainly in the form of oxygen-containing anions (CrO_4^{2-}, $Cr_2O_7^{2-}$), and it can hardly be adsorbed by colloidal substances in the water. Phytoremediation is an effective method in the treatment of heavy metals in soil. Heavy metals can be directly utilized by plants, thus effectively removing heavy metals from soil (Zhou et al., 2018). Adsorption is one of the most effective technologies for the removing heavy metal ions from water (Wang et al., 2018a). Therefore, many materials have been designed and implemented as adsorbents to remove heavy metal from wastewater in academic research and industrial applications (Huang et al., 2015).

Biochar is the product of pyrolysis of biomass at high temperature under anoxic conditions (Huang et al., 2017b; Zhang et al., 2016). There is growing global interest in the role that biochar (BC) play in environmental management (Tan et al., 2015). Biochar could origin from many raw materials, including forest and agricultural waste, industrial by-products and waste, and municipal solid waste (Huang et al., 2017c). Biochar is an attractive carbon-rich material, which has attracted much more attention as a pharmaceutical preparation for water treatment and a soil improvement material (Ding et al., 2016; Tan et al., 2015). The use of biochar can reduce carbon emissions and

* Corresponding author at: College of Environmental Science and Engineering, Hunan University, Changsha, Hunan 410082, China.
E-mail address: huangdanlian@hnu.edu.cn (D. Huang).

https://doi.org/10.1016/j.biortech.2018.12.114
Received 1 November 2018; Received in revised form 27 December 2018; Accepted 30 December 2018
Available online 31 December 2018
0960-8524/

slow down greenhouse effect to a certain extent (Wu et al., 2017). Owning to the excellent performance like its high porosity, large surface area and variable surface composition, biochar has displayed excellent adsorption capacity for pollutants (Wang et al., 2018a). In recent years, many papers have reported the adsorption of pollutants by biochar (Huang et al., 2016a). The ability of biochar to adsorb ionizable antibiotic sulfamethazine was enhanced by addition of carboxyl functionalized short multi-walled carbon nanotubes (Zhang et al., 2016). Biochar can not only be used in water pollution treatment but also in soil and sediment. Composite materials of biochar could immobilize Pb in contaminated sediment (Huang et al., 2018). Due to the limited function of biochar, the application of biochar as adsorbent is limited. Therefore, the functionalization and modification of biochar as an ultrafine composite material is an important topic (Wang et al., 2016).

The chemical composition of layered double hydroxides (LDH) can be represented by the general formula $[M^{2+}_{1-x}M^{3+}_{x}(OH)_2]^{x+}[A^{n-}]_{x/n}{\cdot}mH_2O$, where M^{2+}(Mg^{2+}, Mn^{2+}, Fe^{2+}, Zn^{2+}, Cu^{2+}, etc.) and M^{3+}(Al^{3+}, Fe^{3+}, Co^{3+}, etc.) represent divalent cation and trivalent cation, respectively. A^{n-}(CO_3^{2-}, Cl^-, NO_3^-, citrate, etc.) is an interlayer anion with negative charge, and m represents the number of interlayer water molecules, and × is $M^{2+}/(M^{2+}+M^{3+})$ (Cavani et al., 1991). For high-purity LDH, the value of × is generally from 0.20 to 0.33 (Brindley, 1980). LDH have a certain degree of acidity which depends on the divalent and trivalent metal hydroxides and interlayer anions. At the same time, LDH are alkaline. The alkalinity is related to the nature of divalent and trivalent metal cations (M) and M−O bond on the plates. The anions in the LDH can exchange with other external anions (inorganic anions, organic anions, complex anions, etc.). LDH particles or shaped pieces are limited in the ability to handle contaminants (Cavani et al., 1991). Furthermore, biochar has recently been used as a support framework for nanomaterials, which has the effect of reducing the aggregation of nanomaterials (Huang et al., 2018). LDH have been used to load biochar to improve the ability to remove crystal violet and tetracycline in wastewater (Tan et al., 2016a,b). Cr(VI) mainly exists in the form of anion in water. The application of pure biochar in adsorption of Cr(VI) is scarce.

The objectives of this study were as follows: (1) to synthesize the ethylenediaminetetraacetic acid (EDTA) intercalated Mg/Al-LDH supported biochar (BC@EDTA-LDH) using co-precipitation technique; (2) to analyze the properties of BC@EDTA-LDH using various characterization methods; (3) to study the adsorption performance of BC@EDTA-LDH for Cr(VI); (4) and to explore the adsorption mechanism of BC@EDTA-LDH.

2. Materials and methods

2.1. Materials

The drugs used in the experiment were analytically pure magnesium chloride hexahydrate ($MgCl_2{\cdot}6H_2O$), aluminum chloride hexahydrate ($AlCl_3{\cdot}6H_2O$), sodium hydroxide (NaOH) and disodium edetate (EDTA-2Na), and used. The solution used in the experiment was ultrapure water (resistivity of 18.25 $M\Omega{\cdot}cm^{-1}$), which was also used to rinse and clean the samples. The Cr(VI) stock solution was prepared by dissolving $K_2Cr_2O_7$ in ultrapure water. The desired concentrations of Cr(VI) solution were achieved by the dilution of stock solution. Bamboo biomass was a locally sourced biochar material. The bamboo shavings were cleaned and dried. At last the bamboo shavings were crushed into powder and passed through a 100-mesh sieve.

2.2. Preparation of BC@EDTA-LDH

BC@EDTA-LDH was synthesized by the liquid phase coprecipitation method, and pre-coated on the biomass raw material (bamboo shavings) before pyrolysis (Kameda et al., 2005). The suspension was obtained by immersing bamboo shavings in a mixed solution of $MgCl_2$ and $AlCl_3$ (molar ratio of 3:1) and stirring for 12 h. The solution and suspension were simultaneously and dropwise added to a vessel, maintaining pH at 10 and a stirring speed at 400 r/min. The mixture was stabilized under 60 °C for 12 h. And then, the mixture was filtered and washed three times with ultrapure water and dried. A tube furnace (SK-1200 °C, Tianjin Zhonghuan Experimental Electric Furnace Co., Ltd., China) was used to obtain carbonized biochar. The specimen was heated from room temperature to 480 °C at a rate of 5 °C/min and held for 2 h, in the end, cooled to room temperature, and the product BC@EDTA-LDH was obtained (Rocha et al., 1999; Tan et al., 2016a). BC which was not treated with EDTA-LDH was also produced in the same conditions.

2.3. Characterizations

Brunauer-Emmett-Teller (BET) surface areas of the samples were measured with a Quantachrome Instruments Quadrasorb SI surface area analyzer using BET nitrogen adsorption methods. Fourier transform infrared spectra (FTIR) (Nicolet 5700 Spectrometer, USA) of adsorbent was recorded in the range of 4000–500 cm^{-1}. For purpose of identifying the crystal structure of sample, the X-ray diffraction (XRD) (Bruker D8, German) was performed with diffraction peaks between 5° and 90°. The X-ray photoelectron spectroscopy (XPS) measurement was performed to identify the functional groups on the surface of materials (Thermo ESCALAB 250Xi, USA) with binding energy between 0 and 1400 eV to analyze elemental composition of sample surfaces. The morphological characteristics of samples were obtained using scanning electron microscopy (SEM) (FEI company QUANTA Q400, USA). The point of zero charge of samples was determined for judging the charged condition of the material surface (Zhang et al., 2013).

2.4. Adsorption experiments

The effect of pH on Cr(VI) adsorption was studied in a 20 mL vessel containing 10 mg adsorbent and 10 mL Cr(VI) solution at room temperature (300 ± 0.5 K). The Cr(VI) solution (50 mg/L) was adjusted to 2.0–10.0 using NaOH and HCl solutions. For studying the effect of initial Cr(VI) concentration on Cr(VI) removal, the Cr(VI) solutions with initial concentrations of 20, 50, 70, 100, 150, 200, and 250 mg/L. The impact of ionic strength on Cr(VI) removal was studied with sodium chloride, sodium nitrate and sodium sulfate concentrations varying from 0 to 0.1 M. The pH value of Cr(VI) solution was adjusted to 3, and the mixture was uniformly mixed and shaken for 24 h in a constant-temperature shaking incubator (T = 300 K, r = 180 r/min). The adsorbed samples were filtered through a 0.45 μm filter. The Cr(VI) concentration was determined using a 1,5-diphenylcarbazide spectrophotometric method and the measurement wavelength was 540 nm. And the detection limit was 0.008 mg/L.

In the kinetic experiment, 10 mg adsorbent was added to Cr(VI) solution (50 mg/L at 300 ± 0.5 K). The pH value of Cr(VI) solution was adjusted to 3. Samples were taken at 5, 10, 20, 40, 80, 160, 240, 360, 480, 600, 800, 1200, and 1500 min, and Cr(VI) concentration after reaction was measured.

The removal rate and the adsorption capacity in this study were used to evaluate the material properties. The Cr(VI) removal rate is calculated as follows:

$$\text{Cr(VI)removal rate} = (C_0 - C_e)/C_0 \times 100\% \quad (1)$$

The adsorption capacity (mg/g) is calculated as follows:

$$Q_t=(C_0 - C_e)V/m \quad (2)$$

where C_0 and C_e are the initial and equilibrium concentrations (mg/L) of Cr(VI) respectively, V is the volume of solution (L) and m is the mass of adsorbent (g). All experiments were performed in triplicate, and experimental data was expressed as mean ± deviation.

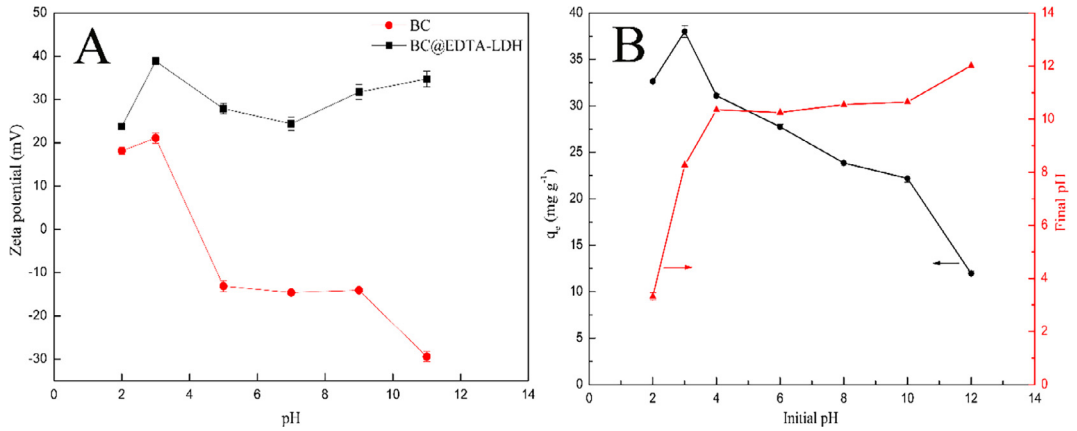

Fig. 1. Zeta potentials of BC and BC@EDTA-LDH at different pH value (A). The effect of initial pH on adsorption capacity and final pH (B). The arrows in this figure represent that the two series of data belong to right-Y axis or left-Y axis, respectively. The error bars represent the standard deviation of the means (n = 3).

3. Results and discussion

3.1. Characterizations

BC had BET surface area of 48.894 m^2/g, and BC@EDTA-LDH had BET surface area of 8.831 m^2/g, which indicated that the voids on the surface of the biochar were filled with the loaded nano-material LDH. After loading the layered double hydroxides, the pores on the biochar were filled, and the BET surface area of the material became smaller. This was further verified by the SEM images (Supplementary material), which exhibited a smooth surface of the original biochar, as opposed to the remarkable roughness on the surface of BC@EDTA-LDH, indicating the formation of sheet LDH on the biochar substrate. Therefore, the synergistic effect of LDH and BC on enhancing Cr(VI) removel could be regarded as an effective matrix for biochar as a dispersed colloid or nano-sized LDH during synthesis, thereby enhancing the active adsorption site of LDH on Cr(VI) aqueous solutions. When the EDTA-Mg/Al LDH was loaded on the surface of bamboo shavings, the layered hexagonal structure could be clearly seen in the SEM images (Supplementary material). After calcination, the original layered structure of bamboo shavings mostly disappeared at temperatures below 500 °C. After adsorption, LDH was reconstructed and $Cr_2O_7^{2-}$ was embedded into the layered structure. Therefore, it could be seen from the SEM images that the layered hexagonal structure appeared after the reaction.

The XRD patterns results for BC, BC@EDTA-LDH and adsorbed BC@EDTA-LDH (BC@EDTA-LDH-Cr) were measured. Some unrecognized peaks appeared in XRD patterns, indicating the unrecognized of other minerals in the bamboo biomass, which were typically detected in biochar produced from plant residues at high pyrolysis temperatures. After high-temperature calcination, the characteristic diffraction peak intensity of BC@EDTA-LDH on the (0 0 3), (0 0 6), (0 0 9), (0 1 0), and (1 1 3) crystal faces remained at a low level. It was proved that the structure of LDH collapsed after high temperature calcination, and the original layered structure changed. The diffraction pattern of BC@EDTA-LDH-Cr showed the layered characteristic diffraction peaks corresponding to (0 0 3), (0 0 6), (0 0 9), (0 1 5), (0 1 2), (1 1 0), and (1 1 3) crystal planes, respectively. Each characteristic peak had high intensity, sharp peak shape and stable baseline (Yang et al., 2002). This proved that water and anions in the reaction system restored the original layered structure by adsorption, indicating that when the material was added to the simulated wastewater, Cr(VI) anion entered the layers of the material and was adsorbed and removed based on the “memory effect” of the material (Cavani et al., 1991).

In the XPS spectra of BC@EDTA-LDH and BC@EDTA-LDH-Cr, the peaks at 285.5 eV and 532.5 eV were corresponding to the spectra of C1s and O1s, respectively (Supplementary material). By comparing the XPS spectra of the material before and after adsorption, it was found that O1s changed significantly. After adsorption, $Cr_2O_7^{2-}$ as interlayer anion entered the recombinant LDH causing increase of the oxygen-containing functional groups. Meanwhile, the peak of Cr appeared at 578 eV. The Cr2p spectra were resolved into three component peaks with binding energy of 573 eV, 578.1 eV and 585.4 eV, which were attached to the Cr, Cr(VI) and Cr(VI), respectively. This indicated that the main removal effect of $Cr_2O_7^{2-}$ was the adsorption of Cr(VI), and proved that $Cr_2O_7^{2-}$ had successfully entered the interlayer of LDH. The increase of H_2O in the XPS C1s peaks after reaction may be due to the presence of bound water in LDH.

The FTIR spectra of materials showed the changes of functional groups (Supplementary material). The broadband of 3643 cm^{-1} was attributed to the –OH tensile vibration, which came from the intermediate layer. In the spectrum of BC@EDTA-LDH and BC@EDTA-LDH-Cr, the peaks at 1193.4 cm^{-1} ascribed to N–H demonstrated the existence of calcination products of EDTA. The FTIR of BC@EDTA-LDH showed C–H bending vibration at 1391 cm^{-1} and C-O bending vibration at 1111 cm^{-1} because of interlayer anion calcination. The FTIR spectra of BC@EDTA-LDH-Cr was related to Cr adsorption at 770 cm^{-1}.

3.2. Effect of solution pH

In the sorption process, pH value is frequently discussed in the influence on the adsorbent surface charge, the ionic state of surface functional groups, and the form of the Cr(VI) species in the adsorption system (Wang et al., 2018a). The influence of initial pH on adsorption capacity and final pH were shown in Fig. 1B. While the pH value increased, the Cr(VI) adsorption capacity by the adsorbent increased at first and then followed by a decrease. It showed that the optimum pH was 3 (Fig. 1B). When the initial pH was between 4.0 and 12.0, the equilibrium pH was at a stable level above 8.0. It could be explained that LDH had cushioning properties (Seida and Nakano, 2000; Wang et al., 2018b). The zeta potential of BC@EDTA-LDH was shown in Fig. 1A. At different pH values, zeta potential of BC@EDTA-LDH was positive. That was to say, the surface of the material was always positively charged, resulting in electrostatic attraction between the material and the $Cr_2O_7^{2-}$ ion. With the increase of pH, the adsorption capacity decreased, which may be due to the enhancement of the electrostatic repulsion between $Cr_2O_7^{2-}$ and OH^- and the competition for adsorption sites. The results showed that adsorption behavior of adsorbent on Cr(VI) significantly related to the pH of the solution.

3.3. Adsorption kinetics

Kinetic experiments show that Cr(VI) adsorption by BC@EDTA-LDH increased rapidly with time. During the first four hours, the adsorption

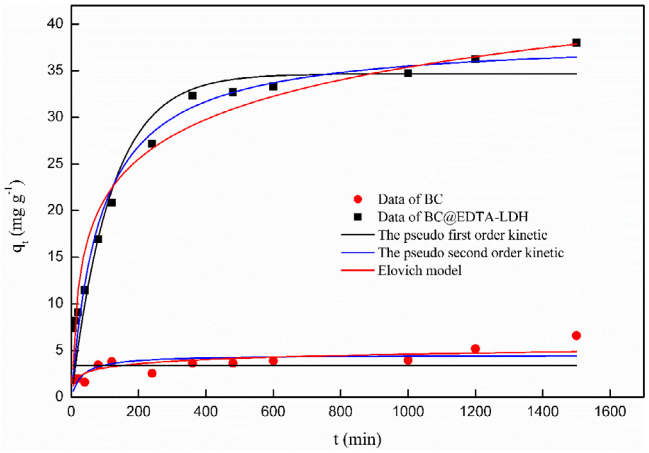

Fig. 2. Adsorption kinetics of Cr(VI) on BC and BC@EDTA-LDH.

capacity increased rapidly and reached 27 mg/g due to the large amount of adsorption and reached equilibrium in about 24 h (Fig. 2). The adsorption capacity remained stable over time which may be because the adsorption site has already been occupied.

The pseudo first order model, pseudo second order model, and Elovich model were applied to simulate the experimental kinetic data. These three models can be represented by the following equation:

$$\frac{dq_t}{dt}=k_1(q_e - q_t) \quad (3)$$

$$\frac{dq_t}{dt} = k_2(q_e - q_t)^2 \quad (4)$$

$$\frac{dq_t}{dt} = \alpha \exp(-\beta q_t) \quad (5)$$

where q_t and q_e are the quantity of Cr(VI) adsorbed at time t and equilibrium (mg/g); k_1 and k_2 are primary and secondary apparent adsorption rate constants (h^{-1} and $g{\cdot}mg^{-1}{\cdot}h^{-1}$, respectively); α is the initial adsorption rate (mg/g); β is the desorption constant (g/mg). Table 1 gives the model parameters for the first-order, second-order and Elovich models of the fitted experimental data. Based on the evaluation of the coefficient of determination (R^2), it showed that second-order model was the well-suited one to describe the adsorption kinetics. This could be further confirmed by the well agreement between the calculated $q_{e,cal}$ value and the experimental results. This could be explained that chemisorption was the rate limiting step. The removal of Cr(VI) may cause electron transfer between material and Cr(VI). Other studies had reported similar results (Tan et al., 2016b). The correlation coefficient of the Elovich model ($R^2 > 0.95$) was a good description of the results, indicating that Cr(VI) adsorption on BC@EDTA-LDH was heterogeneously diffused.

3.4. Adsorption isotherms

The three isotherm models of Langmuir, Freundlich and Langmuir-Freundlich were imitate for simulating the adsorption of Cr(VI) on BC@EDTA-LDH:

$$q_e=\frac{K_L Q C_e}{1+KC_e} \quad (6)$$

$$q_e=K_F C_e^n \quad (7)$$

$$q_e=\frac{KQC_e^n}{1+KC_e^n} \quad (8)$$

where K_L, K_F and K represent constants connected with the affinity of adsorbent binding site; Q is the saturated adsorption amount (mg/g), which indicates the quantity of adsorption onto the surface of unit adsorbent; C_e is equilibrium solution concentration. n is Freundlich linear constant: the smaller the n is, the better the adsorption performance is; it is generally considered to be easy to adsorb at 0.1–0.5; when it is greater than 2, it is difficult to adsorb. The Langmuir model assumes that a single layer is adsorbed on a uniform surface and there is no interaction on the adsorbent. However, Freundlich and Langmuir-Freundlich models are empirical formulas that are commonly used to depict chemisorption on heterogeneous surfaces.

These three models can reproduce the experimental data properly (Fig. 3). The correlation coefficients between the simulated values and the measured values of the Langmuir model and the Langmuir-Freundlich model were higher than 0.9 (Table 1), which reflected the isotherm data reasonably well. The stability constant of the Langmuir model was 0.29, indicating the adsorption of Cr(VI) was favorable ($0 < K_L < 1$), and the sorption process may be a uniform monolayer sorption process. The adsorption capacity of BC@EDTA-LDH increased rapidly with the raising of initial concentration. This phenomenon testified that Cr(VI) was driven to surface of BC@EDTA-LDH at high concentrations. The adsorption then became stable and reached equilibrium. The maximum adsorption capacity of Langmuir for BC@EDTA-LDH composites was 52.22 mg/g, while the maximum adsorption capacity of Langmuir-Freundlich was 55.19 mg/g, which was higher than some previously reported biochar adsorbents. The R^2 of these models were not much different, indicating that Cr(VI) adsorption on BC@EDTA-LDH can be regulated by multiple processes. This suggested that surface adsorption and interlayer anion exchanges determined the adsorption of Cr(VI).

3.5. Effect of coexisting anions

In the actual industrial wastewater and contaminated natural water, there are many kinds of pollutants. The presence of these soluble ions may have a competitive effect on the adsorption site and influence the Cr(VI) adsorption. Therefore, this section studied the impact of coexisting anions on Cr(VI) removal by BC@EDTA-LDH. The influence of

Table 1
The model parameters of adsorption kinetics and adsorption isotherms.

Model/equations	Sorbents	Parameter 1	Parameter 2	R^2
Pseudo first order kinetic	BC	$q_{e,cal}$ = 3.40 (mg/g)	k_1 = 0.019 h^{-1}	0.61
	BC@EDTA-LDH	$q_{e,cal}$ = 34.67 (mg/g)	k_1 = 0.0085 h^{-1}	0.93
Pseudo second order kinetic	BC	$q_{e,cal}$ = 4.52 (mg/g)	k_2 = 0.0072 kg g^{-1} h^{-1}	0.48
	BC@EDTA-LDH	$q_{e,cal}$ = 37.88 (mg/g)	k_2 = 0.00030 kg g^{-1} h^{-1}	0.96
Elovich model	BC	α = 0.88 g/kg	β = 1.57 g/kg	0.67
	BC@EDTA-LDH	α = 1.99 g/kg	β = 0.16 g/kg	0.95
Langmuir	BC	K_L = 0.003 L/mg	Q = 18.45 mg/g	0.94
	BC@EDTA-LDH	K_L = 0.29 L/mg	Q = 52.22 mg/g	0.97
Freundlich	BC	K_F = 0.14 L/mg	n = 0.73	0.94
	BC@EDTA-LDH	K_F = 23.49 L/mg	n = 0.16	0.85
Langmuir–Freundlich	BC	K = 0.003 L/mg	Q = 27.79 mg/g	0.93
	BC@EDTA-LDH	K = 0.35 L/mg	Q = 55.19 mg/g	0.98

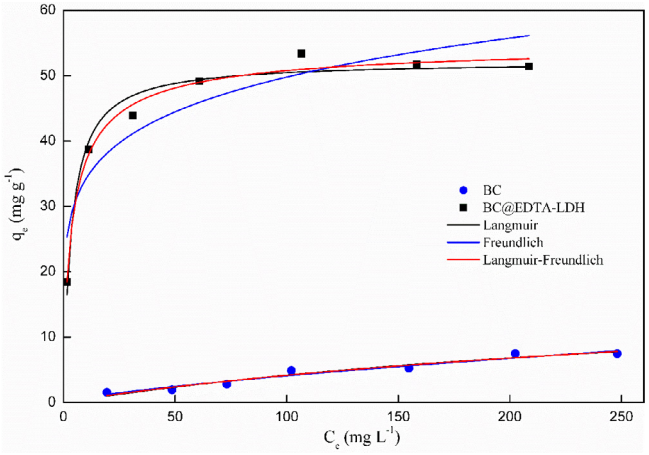

Fig. 3. Adsorption isotherms of Cr(VI) on BC and BC@EDTA-LDH.

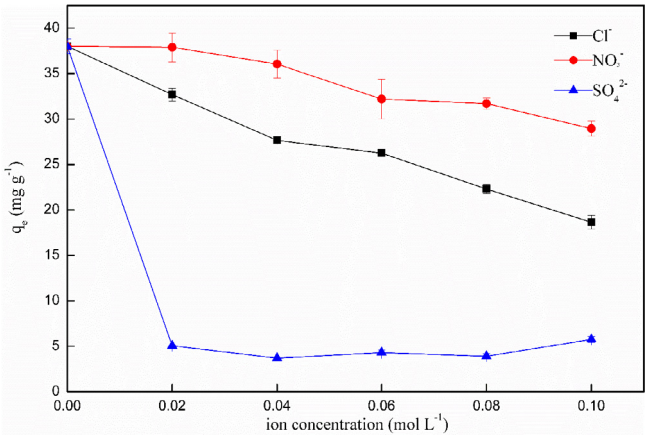

Fig. 4. The effect of ionic strength on the Cr(VI) adsorption capacity of BC@EDTA-LDH. The error bars represent the standard deviation of the means (n = 3).

coexisting anions on Cr(VI) adsorption was shown in Fig. 4. The concentrations of sodium chloride, sodium nitrate and sodium sulfate varied between 0 and 0.1 M. Fig. 4 showed that the impact of nitrate on the Cr(VI) removal efficiency was relatively low, and the low concentration of sulfate could have a large influence on the Cr(VI) removal by BC@EDTA-LDH. Although the interference of competitive anions on adsorption of Cr(VI) by BC@EDTA-LDH follows the order of SO_4^{2-} > Cl^- > NO_3^-, the coulomb interaction of anions exchange sites on the LDH could not account for these uncommon anions exchange. Generally, in the oxygen anion adsorption of LDH, higher valence anions had more significant interference effects than monovalent anions (Goh et al., 2008). The size of the interlayer space during anion exchange limited the anion, which also explained the selectivity of the adsorbent to contaminants (Xue et al., 2016). In general, the replacement anion had a small anion radius, the negative charge carrying capacity was low, and the replacement performance was stronger. Thus, the amount of charge carried by Cl^- and NO_3^- was lower than that of $Cr_2O_7^{2-}$, so the stability of LDH formed by recombination was relatively high, which indicated that it could not easily be replaced by Cl^- and NO_3^-. The amount of charge carried by SO_4^{2-} was the same as that of $Cr_2O_7^{2-}$, so it had a great influence on the Cr(VI) removal (Goh et al., 2008; Miyata, 1983).

3.6. Adsorption mechanisms

According to the structure and adsorption properties of the material, the possible adsorption mechanism of the material was obtained. The results of BET surface area measurement showed that the specific surface area of BC@EDTA-LDH was significantly lower than BC. The reason was that the bamboo shavings loaded with LDH were calcined to obtain a new material BC@LDH with a large number of bimetallic oxides on the surface. Comparing the BET surface area of BC@EDTA-LDH and BC, it indicated that the Cr(VI) removal by BC@EDTA-LDH did not solely lie on its pore structure and that new layered double hydroxides intercalated with $Cr_2O_7^{2-}$ may be the pivotal position in Cr (VI) removal. Biochar was used as a support framework for nanomaterials, which had the effect of reducing the aggregation of nanomaterials. Calcined EDTA-Mg/Al LDH had the property of reconstructing into layered double hydroxide structure ("memory effect") (El Gaini et al., 2009; Tan et al., 2016b). If the calcination temperature is too high, the decomposition products cannot be restored to the layered structure of LDH (Chagas et al., 2015). EDTA did not exist on BC@EDTA-LDH after calcination. After EDTA was pyrolyzed, it will not compete with $Cr_2O_7^{-2}$ in the sorption process. The FTIR spectra of BC@EDTA-LDH-Cr confirmed the reconstruction of the calcined LDH intercalated with Cr(VI). The XRD pattern of BC@EDTA-LDH-Cr also showed the characteristic difference of LDH, demonstrating that Mg/Al-LDH was reconstituted owing to the adsorption. During the reconstruction process, the anion was embedded in the layered structure and the OH^- was simultaneously released. The initial and final pH of Cr(VI) solutions were shown in Fig. 1B. Fig. 1B showed that the final pH was significantly increased to 10–12.02.

Previous studies had attributed Cr(VI) adsorption of layered double hydroxides to surface adsorption, interlayer anion exchange and precipitation, relating to reaction time, solution concentration, LDH type and solution pH value. To determine the effect of solution pH, the results of Cr(VI) removal at different pH values were measured, and the pH of solution after adsorption was examined. The final pH may be associated with LDH dissolution. Therefore, the change of pH with the reaction time can well indicate that chemical adsorption process was the primary controlling factor for Cr(VI) removal by BC@EDTA-LDH, which was consistent with the results of second-order kinetic.

4. Conclusions

BC@EDTA-LDH could be produced by liquid phase coprecipitation of LDH on biochar substrates, providing an efficient adsorbent to remove Cr(VI) in aqueous solutions. The experimental results demonstrated that interlayer anion exchange and surface adsorption dominated Cr(VI) sorption process. The pseudo second-order and Langmuir-Freundlich models were well-fitted the sorption process, indicating chemisorption and monolayer adsorption were the main mechanisms of the adsorption. Since biochar was prepared from low-cost agricultural waste, the use of biochar as a carrier for LDH was environmentally friendly. Further studies on the use of BC@EDTA-LDH in wastewater can be investigated in the future.

Acknowledgments

This study was financially supported by the Program for the National Natural Science Foundation of China (51879101, 51579098, 51779090, 51709101, 51521006, 51809090, 51278176, 51378190), the National Program for Support of Top–Notch Young Professionals of China (2014), the Program for Changjiang Scholars and Innovative Research Team in University (IRT-13R17), and Hunan Provincial Science and Technology Plan Project (2018SK20410, 2017SK2243, 2016RS3026), and the Fundamental Research Funds for the Central Universities (531109200027, 531107051080, 531107050978).

Competing interests statement

We declared that we have no competing interests.

Appendix A. Supplementary data

Supplementary data to this article can be found online at https://doi.org/10.1016/j.biortech.2018.12.114.

References

Brindley, G.W., 1980. Thermal behavior of hydrotalcite and of anion-exchanged forms of hydrotalcite. Clays Clay Miner. 28 (2), 87–91.

Cavani, F., Trifirò, F., Vaccari, A., 1991. Hydrotalcite-type anionic clays: preparation, properties and applications. ChemInform 23 (12), 173–298.

Chagas, L.H., De Carvalho, G.S.G., Do Carmo, W.R., San Gil, R.A.S., Chiaro, S.S.X., Leitão, A.A., Diniz, R., De Sena, L.A., Achete, C.A., 2015. MgCoAl and NiCoAl LDHs synthesized by the hydrothermal urea hydrolysis method: structural characterization and thermal decomposition. Mater. Res. Bull. 64, 207–215.

Ding, Y., Liu, Y., Liu, S., Li, Z., Tan, X., Huang, X., Zeng, G., Zhou, L., Zheng, B., 2016. Biochar to improve soil fertility. a review. Agronomy Sust. Dev. 36 (2), 1–18.

El Gaini, L., Lakraimi, M., Sebbar, E., Meghea, A., Bakasse, M., 2009. Removal of indigo carmine dye from water to Mg-Al-CO(3)-calcined layered double hydroxides. J. Hazard Mater. 161 (2–3), 627–632.

Farrell, R.P., Judd, R.J., Lay, P.A., Dixon, N.E., Baker, R.S., Bonin, A.M., 1989. Chromium (V)-induced cleavage of DNA: are chromium(V) complexes the active carcinogens in chromium(VI)-induced cancers? Chem. Res. Toxicol. 2 (4), 227–229.

Fendorf, S., Wielinga, B.W., Hansel, C.M., 2000. Chromium transformations in natural environments: the role of biological and abiological processes in chromium(VI) reduction. Int. Geol. Rev. 42 (8), 691–701.

Goh, K.H., Lim, T.T., Dong, Z., 2008. Application of layered double hydroxides for removal of oxyanions: a review. Water Res. 42 (6–7), 1343–1368.

Gong, X., Huang, D., Liu, Y., Zeng, G., Wang, R., Wan, J., Zhang, C., Cheng, M., Qin, X., Xue, W., 2017. Stabilized nanoscale zerovalent iron mediated cadmium accumulation and oxidative damage of Boehmeria nivea (L.) gaudich cultivated in cadmium contaminated sediments. Environ. Sci. Technol. 51 (19), 11308–11316.

Gong, X., Huang, D., Liu, Y., Zeng, G., Wang, R., Wei, J., Huang, C., Xu, P., Wan, J., Zhang, C., 2018. Pyrolysis and reutilization of plant residues after phytoremediation of heavy metals contaminated sediments: for heavy metals stabilization and dye adsorption. Bioresour. Technol. 253, 64–71.

He, H., Xiang, Z., Chen, H., Chen, X., Huang, H., Wen, M., Yang, C., 2018. Biosorption of Cd(II) from synthetic wastewater using dry biofilms from biotrickling filters. Int. J. Environ. Sci. Technol. 15 (7), 1491–1500.

Huang, D., Deng, R., Wan, J., Zeng, G., Xue, W., Wen, X., Zhou, C., Hu, L., Liu, X., Xu, P., Guo, X., Ren, X., 2018. Remediation of lead-contaminated sediment by biochar-supported nano-chlorapatite: accompanied with the change of available phosphorus and organic matters. J. Hazard. Mater. 348, 109–116.

Huang, D., Hu, C., Zeng, G., Cheng, M., Xu, P., Gong, X., Wang, R., Xue, W., 2017a. Combination of Fenton processes and biotreatment for wastewater treatment and soil remediation. Sci. Total Environ. 574, 1599–1610.

Huang, D., Liu, L., Zeng, G., Xu, P., Huang, C., Deng, L., Wang, R., Wan, J., 2017b. The effects of rice straw biochar on indigenous microbial community and enzymes activity in heavy metal-contaminated sediment. Chemosphere 174, 545–553.

Huang, D., Wang, X., Zhang, C., Zeng, G., Peng, Z., Zhou, J., Cheng, M., Wang, R., Hu, Z., Qin, X., 2017c. Sorptive removal of ionizable antibiotic sulfamethazine from aqueous solution by graphene oxide-coated biochar nanocomposites: influencing factors and mechanism. Chemosphere 186, 414–421.

Huang, D., Wang, Y., Zhang, C., Zeng, G., Lai, C., Wan, J., Qin, L., Zeng, Y., 2016a. Influence of morphological and chemical features of biochar on hydrogen peroxide activation: implications on sulfamethazine degradation. Rsc Adv. 6 (77), 73186–73196.

Huang, D., Xue, W., Zeng, G., Wan, J., Chen, G., Huang, C., Zhang, C., Cheng, M., Xu, P., 2016b. Immobilization of Cd in river sediments by sodium alginate modified nanoscale zero-valent iron: Impact on enzyme activities and microbial community diversity. Water Res. 106, 15–25.

Huang, D.L., Wang, R.Z., Liu, Y.G., Zeng, G.M., Lai, C., Xu, P., Lu, B.A., Xu, J.J., Wang, C., Huang, C., 2015. Application of molecularly imprinted polymers in wastewater treatment: a review. Environ. Sci. Pollut. Res. 22 (2), 963–977.

Kameda, T., Saito, S., Umetsu, Y., 2005. Mg-Al layered double hydroxide intercalated with ethylene-diaminetetraacetate anion: Synthesis and application to the uptake of heavy metal ions from an aqueous solution. Separat. Purificat. Technol. 47 (1), 20–26.

Knott, M., 1996. Toxic tannery sludge made as safe as houses. New Scient. 149 (2017), 22.

Li, X., Yang, W.L., He, H., Wu, S., Zhou, Q., Yang, C., Zeng, G., Luo, L., Lou, W., 2018. Responses of microalgae Coelastrella sp. to stress of cupric ions in treatment of anaerobically digested swine wastewater. Bioresour. Technol. 251, 274–279.

Miyata, S., 1983. Anion-exchange properties of hydrotalcite-like compounds. Clays Clay Miner. 31 (4), 305–311.

Rocha, J., Arco, M.D., Rives, V.A., Ulibarri, M.A., 1999. Reconstruction of layered double hydroxides from calcined precursors: a powder XRD and 27A1 MAS NMR study. J. Mater. Chem. 9 (10), 2499–2503.

Seida, Y., Nakano, Y., 2000. Removal of humic substances by layered double hydroxide containing iron. Water Res. 34 (5), 1487–1494.

Tan, X., Liu, S., Liu, Y., Gu, Y., Zeng, G., Cai, X., Yan, Z., Yang, C., Hu, X., Chen, B., 2016a. One-pot synthesis of carbon supported calcined-Mg/Al layered double hydroxides for antibiotic removal by slow pyrolysis of biomass waste. Sci. Rep. 6, 39691.

Tan, X., Liu, Y., Zeng, G., Wang, X., Hu, X., Gu, Y., Yang, Z., 2015. Application of biochar for the removal of pollutants from aqueous solutions. Chemosphere 125, 70–85.

Tan, X.F., Liu, Y.G., Gu, Y.L., Liu, S.B., Zeng, G.M., Cai, X., Hu, X.J., Wang, H., Liu, S.M., Jiang, L.H., 2016b. Biochar pyrolyzed from MgAl-layered double hydroxides pre-coated ramie biomass (Boehmeria nivea (L.) Gaud.): characterization and application for crystal violet removal. J. Environ. Manage. 184 (Pt 1), 85–93.

Wang, R.Z., Huang, D.L., Liu, Y.G., Zhang, C., Lai, C., Zeng, G.M., Cheng, M., Gong, X.M., Wan, J., Luo, H., 2018a. Investigating the adsorption behavior and the relative distribution of Cd(2+) sorption mechanisms on biochars by different feedstock. Bioresour. Technol. 261, 265–271.

Wang, S., Gao, B., Li, Y., Zimmerman, A., Cao, X., 2016. Sorption of arsenic onto Ni/Fe layered double hydroxide (LDH)-biochar composites. Rsc Adv. 6 (22), 17792–17799.

Wang, T., Li, C., Wang, C., Wang, H., 2018b. Biochar/MnAl-LDH composites for Cu (II) removal from aqueous solution. Coll. Surf. A: Physicochem. Eng. Asp. 538, 443–450.

Wang, Y.T., Chirwa, E.M., Shen, H., 2000. Cr(VI) Reduction in continuous-flow coculture bioreactor. J. Environ. Eng. 126 (4), 300–306.

Wu, S., He, H., Inthapanya, X., Yang, C., Lu, L., Zeng, G., Han, Z., 2017. Role of biochar on composting of organic wastes and remediation of contaminated soils-a review. Environ. Sci. Pollut. Res. Int. 24 (20), 16560–16577.

Xu, Y., Zhao, D., 2007. Reductive immobilization of chromate in water and soil using stabilized iron nanoparticles. Water Res. 41 (10), 2101–2108.

Xue, L., Gao, B., Wan, Y., Fang, J., Wang, S., Li, Y., Muñoz-Carpena, R., Yang, L., 2016. High efficiency and selectivity of MgFe-LDH modified wheat-straw biochar in the removal of nitrate from aqueous solutions. J. Taiwan Instit. Chem. Eng. 63, 312–317.

Xue, W., Huang, D., Zeng, G., Wan, J., Zhang, C., Xu, R., Cheng, M., Deng, R., 2017. Nanoscale zero-valent iron coated with rhamnolipid as an effective stabilizer for immobilization of Cd and Pb in river sediments. J. Hazard. Mater. 341, 381–389.

Yang, W., Kim, Y., Liu, P.K.T., Sahimi, M., Tsotsis, T.T., 2002. A study by in situ techniques of the thermal evolution of the structure of a Mg–Al–CO 3 layered double hydroxide. Chem. Eng. Sci. 57 (15), 2945–2953.

Zhang, C., Lai, C., Zeng, G., Huang, D., Yang, C., Wang, Y., Zhou, Y., Cheng, M., 2016. Efficacy of carbonaceous nanocomposites for sorbing ionizable antibiotic sulfamethazine from aqueous solution. Water Res. 95, 103–112.

Zhang, M., Gao, B., Yao, Y., Inyang, M., 2013. Phosphate removal ability of biochar/MgAl-LDH ultra-fine composites prepared by liquid-phase deposition. Chemosphere 92 (8), 1042–1047.

Zhou, Q., Lin, Y., Li, X., Yang, C., Han, Z., Zeng, G., Lu, L., He, S., 2018. Effect of zinc ions on nutrient removal and growth of Lemna aequinoctialis from anaerobically digested swine wastewater. Bioresour. Technol. 249, 457–463.